LETTER

doi:10.1038/nature21426

Observation of discrete time-crystalline order in a disordered dipolar many-body system

Soonwon Choi[1]*, Joonhee Choi[1,2]*, Renate Landig[1]*, Georg Kucsko[1], Hengyun Zhou[1], Junichi Isoya[3], Fedor Jelezko[4], Shinobu Onoda[5], Hitoshi Sumiya[6], Vedika Khemani[1], Curt von Keyserlingk[7], Norman Y. Yao[8], Eugene Demler[1] & Mikhail D. Lukin[1]

Understanding quantum dynamics away from equilibrium is an outstanding challenge in the modern physical sciences. Out-of-equilibrium systems can display a rich variety of phenomena, including self-organized synchronization and dynamical phase transitions[1,2]. More recently, advances in the controlled manipulation of isolated many-body systems have enabled detailed studies of non-equilibrium phases in strongly interacting quantum matter[3–6]; for example, the interplay between periodic driving, disorder and strong interactions has been predicted to result in exotic 'time-crystalline' phases[7], in which a system exhibits temporal correlations at integer multiples of the fundamental driving period, breaking the discrete time-translational symmetry of the underlying drive[8–12]. Here we report the experimental observation of such discrete time-crystalline order in a driven, disordered ensemble of about one million dipolar spin impurities in diamond at room temperature[13–15]. We observe long-lived temporal correlations, experimentally identify the phase boundary and find that the temporal order is protected by strong interactions. This order is remarkably stable to perturbations, even in the presence of slow thermalization[16,17]. Our work opens the door to exploring dynamical phases of matter and controlling interacting, disordered many-body systems[18–20].

Conventional wisdom holds that the periodic driving of isolated, interacting systems inevitably leads to heating and the loss of quantum coherence. In certain cases, however, fine-tuned driving can actually decouple quantum degrees of freedom from both their local environment[14] and each other[21]. Recently, it has been shown that strong disorder, which leads to many-body localization[22,23], allows a system to retain memory of its initial state for long times, enabling the observation of novel, out-of-equilibrium quantum phases[3,5,24]. One example is the discrete time crystal[9–12]—a phase that is nominally forbidden in equilibrium[25,26]. The essence of the discrete time-crystalline (DTC) phase is an emergent, collective, subharmonic temporal response. Although this phenomenon resembles the coherent revivals associated with dynamical decoupling[13], its nature is fundamentally different because it is induced and protected by interactions rather than by fine-tuned control fields. It is especially intriguing to investigate the possibility of DTC order in systems that are not obviously localized[27]. This is the case for dipolar spins in three dimensions, where the interplay between interactions and disorder can lead to critical subdiffusive dynamics[17,28].

We experimentally investigate the formation of DTC order in an ensemble of nitrogen–vacancy spin impurities in diamond. Each nitrogen–vacancy centre has an electronic $S=1$ spin, from which we isolate an effective two-level system by applying an external magnetic field. These isolated spin states can be optically initialized, detected and manipulated via microwave radiation[13,15] (see Fig. 1a and Methods). Our sample has a high concentration (45 p.p.m.) of nitrogen–vacancy centres, giving rise to strong long-range magnetic dipolar interactions[17]. The spins are also subject to multiple sources of disorder, owing to lattice strain, paramagnetic impurities and the random positioning of nitrogen–vacancy centres. A strong, resonant microwave field is used to control spin orientations, resulting in an effective Hamiltonian (in the rotating frame)[17]

$$H(t)=\sum_i \Omega_x(t)S_i^x+\Omega_y(t)S_i^y+\Delta_i S_i^z + \sum_{ij}\left(J_{ij}/r_{ij}^3\right)\left(S_i^xS_j^x+S_i^yS_j^y-S_i^zS_j^z\right)$$

Here, S_i^μ ($\mu\in\{x,y,z\}$) are Pauli spin-1/2 operators acting on the effective two-level system spanned by the spin states $|m_s=0\rangle$ and $|m_s=-1\rangle$, $\Omega_{x(y)}$ is the Rabi frequency of the microwave driving, Δ_i is a disordered on-site field with approximate standard deviation $W=2\pi\times 4.0\,\mathrm{MHz}$, r_{ij} is the distance between spins i and j (average nearest-neighbour separation $r_0\approx 8\,\mathrm{nm}$), and J_{ij} are the orientation-dependent coefficients of the dipolar interaction. The average interaction, $J_{ij}/r_0^3\approx 2\pi\times 105\,\mathrm{kHz}$ (ref. 17), is much faster than typical spin coherence times[15].

To probe the existence of time-crystalline order, we monitor the spin dynamics of an initial state that is polarized along the $+\hat{x}$ direction. We begin by applying continuous microwave driving (spin locking) along $\hat{x}$ with Rabi frequency $\Omega_x=2\pi\times 54.6\,\mathrm{MHz}$ for a duration τ_1 (Fig. 1a). Next, we rotate the spin ensemble by an angle θ around the $\hat{y}$ axis using a strong microwave pulse with $\Omega_y=2\pi\times 41.7\,\mathrm{MHz}$ for duration $\tau_2=\theta/\Omega_y\ll\tau_1$. This two-step sequence defines a Floquet unitary with a total period $T=\tau_1+\tau_2$, and is repeated n times before the polarization $P(nT)$ along the $\hat{x}$ axis is measured. The resulting polarization dynamics are analysed in both the time and frequency (ν) domain. Repeating these measurements with various values of τ_1 and θ allows us to independently explore the effect of interactions and global rotations.

Figure 1b–d depicts representative time traces and the corresponding Fourier spectra, $S(\nu)\equiv\sum_n P(nT)\mathrm{e}^{i2\pi n\nu}$, for various values of τ_1 and θ. For relatively short interaction times ($\tau_1=92\,\mathrm{ns}$) and nearly perfect π pulses ($\theta\approx\pi$), we observe that the spin polarization $P(nT)$ alternates between positive and negative values, resulting in a subharmonic peak at $\nu=1/2$ (Fig. 1b). In our experiment, the microwave pulses have an intrinsic uncertainty of 0.9% stemming from a combination of spatial inhomogeneity in the microwave fields, on-site potential disorder and the effect of dipolar interactions (see Methods). These effects eventually

[1]Department of Physics, Harvard University, Cambridge, Massachusetts 02138, USA. [2]School of Engineering and Applied Sciences, Harvard University, Cambridge, Massachusetts 02138, USA. [3]Research Centre for Knowledge Communities, University of Tsukuba, Tsukuba, Ibaraki 305-8550, Japan. [4]Institut für Quantenoptik and Center for Integrated Quantum Science and Technology, Universität Ulm, 89081 Ulm, Germany. [5]Takasaki Advanced Radiation Research Institute, National Institutes for Quantum and Radiological Science and Technology, 1233 Watanuki, Takasaki, Gunma 370-1292, Japan. [6]Sumitomo Electric Industries Ltd, Itami, Hyougo 664-0016, Japan. [7]Princeton Center for Theoretical Science, Princeton University, Princeton, New Jersey 08544, USA. [8]Department of Physics, University of California Berkeley, Berkeley, California 94720, USA.
*These authors contributed equally to this work.

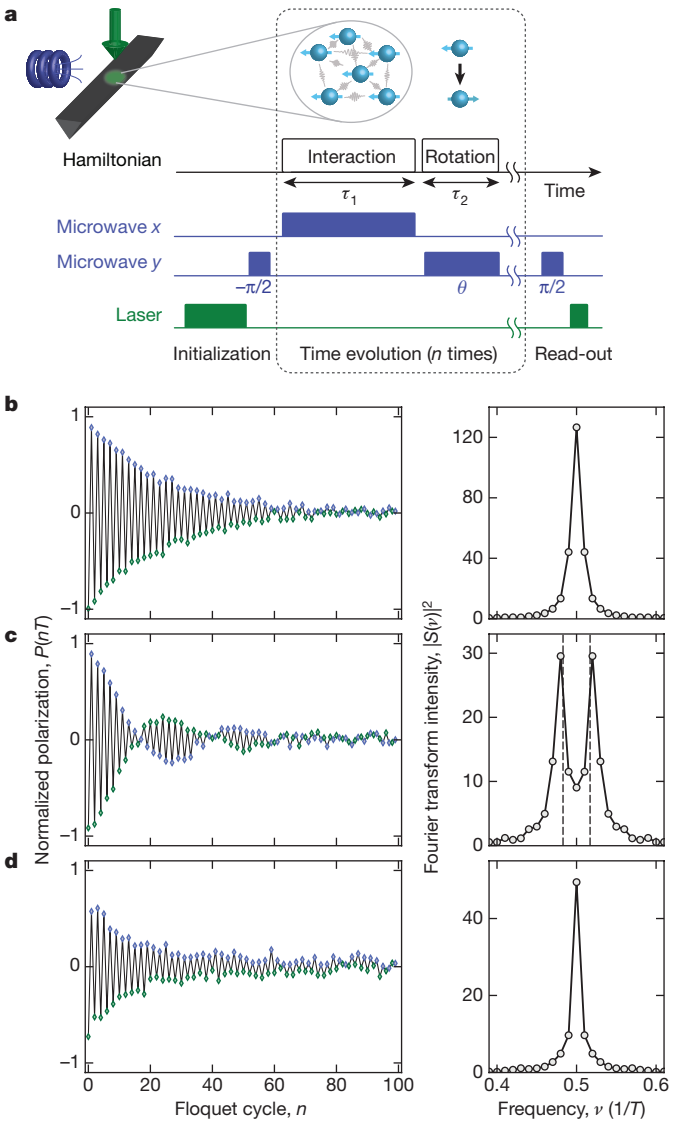

Figure 1 | Experimental set-up and observation of discrete time-crystalline order. **a**, Nitrogen–vacancy centres (blue spheres) in a nanobeam fabricated from black diamond are illuminated by a focused green laser beam and irradiated by a microwave source. Spins are prepared in the $(|m_s{=}0\rangle + |m_s{=}-1\rangle)/\sqrt{2}$ state using a microwave $-\pi/2$ pulse along the $\hat{y}$ axis. Subsequently, within one Floquet cycle, the spins evolve under a dipolar interaction and microwave field Ω_x aligned along the $\hat{x}$ axis for duration τ_1, immediately followed by a global microwave θ pulse along the $\hat{y}$ axis. After n repetitions of the Floquet cycle, the spin polarization along the $\hat{x}$ axis is read out. We choose τ_1 to be an integer multiple of $2\pi/\Omega_x$ to minimize accidental dynamical decoupling[14]. **b**–**d**, Representative time traces of the normalized spin polarization $P(nT)$ measured at even (green) and odd (blue) integer multiples of T, and respective Fourier spectra $|S(\nu)|^2$ for different values of the interaction time τ_1 and θ: $\tau_1 = 92$ ns, $\theta = \pi$ (**b**); $\tau_1 = 92$ ns, $\theta = 1.034\pi$ (**c**); and $\tau_1 = 989$ ns, $\theta = 1.034\pi$ (**d**). Dashed lines in **c** indicate $\nu = 1/2 \pm (\theta - \pi)/(2\pi)$. Data are averaged over more than 2×10^4 measurements.

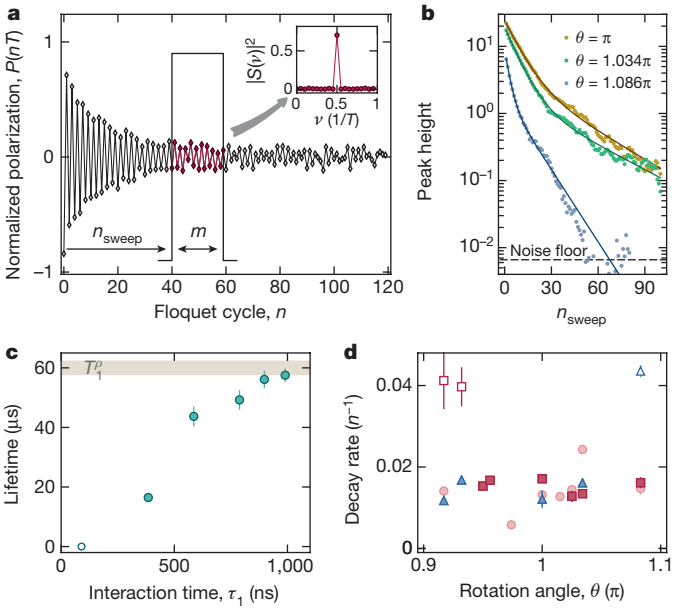

Figure 2 | Long-time behaviour of discrete time-crystalline order. **a**, Representative time trace of the normalized spin polarization $P(nT)$ in the crystalline phase ($\tau_1 = 790$ ns and $\theta = 1.034\pi$). The time-dependent intensity of the $\nu = 1/2$ peak (inset) is extracted from a short-time Fourier transformation with a time window of length $m = 20$ shifted from the origin by n_{sweep}. **b**, Peak height at $\nu = 1/2$ as a function of n_{sweep} for different pulse imperfections at $\tau_1 = 790$ ns. Lines indicate fits to the data using a phenomenological double-exponential function. The noise floor corresponds to 0.017, which is extracted from the mean value plus the standard deviation of $\sum_\nu |S(\nu)|^2$, excluding the $\nu = 1/2$ peak. **c**, Extracted lifetime of the time-crystalline order as a function of the interaction time τ_1, for $\theta = 1.034\pi$. The shaded region indicates the spin lifetime $T_1^\rho = 60 \pm 2$ μs (extracted from a stretched exponential[28]) due to coupling with the external environment. **d**, Extracted decay rate of the time-crystalline order (in Floquet units) as a function of θ for different interaction times: $\tau_1 = 385$ ns (circles), 586 ns (squares) and 788 ns (triangles). Only very weak dependence on $\theta - \pi$ is observed within the DTC phase, contrary to a dephasing model (Methods). In **c** and **d**, the vertical error bars display the statistical error (s.d.) from the fit and empty symbols mark data near the time-crystalline phase boundary.

cause the oscillations to decay, after approximately 50 periods. Although such temporal oscillations nominally break discrete time-translation symmetry, their physical origin is trivial. To see this, we note that for sufficiently strong microwave driving, $\Omega_x \gg W, J_{ij}/r_0^3$, the dynamics during τ_1 are governed by an effective polarization-conserving Hamiltonian[17], $H_{\text{eff}} \approx \sum_i \Omega_x S_i^x + \sum_{ij} \left(J_{ij}/r_{ij}^3\right) S_i^x S_j^x$. During τ_2, the evolution can be approximated as a global spin rotation $R_y^\theta \approx \exp(-i\theta \sum_i S_i^y)$. When $\theta = \pi$, this pulse simply flips the sign of the $\hat{x}$ polarization during each Floquet cycle, resulting in the $\nu = 1/2$ peak. However, this $2T$-periodic response originates from the fine tuning of θ and should not be robust against perturbations. Indeed, a systematic change in the average rotation angle to $\theta = 1.034\pi$ causes the $2T$-periodicity to completely disappear, resulting in a modulated, decaying signal with two incommensurate Fourier peaks at $\nu = 1/2 \pm (\theta - \pi)/(2\pi)$ (Fig. 1c). Remarkably, we find that a rigid $2T$-periodic response is restored when interactions are enhanced by increasing τ_1 to 989 ns, suggesting that the $\nu = 1/2$ peak is stabilized by interactions. In this case, we observe a sharp peak in the spectrum at $\nu = 1/2$ and the oscillations in $P(nT)$ continue beyond $n \approx 100$ (Fig. 1d), indicating a persistent subharmonic temporal response.

The robustness of this apparent periodic order is further explored in Fig. 2. With an interaction time $\tau_1 = 790$ ns and $\theta = 1.034\pi$, the polarization exhibits an initial decay followed by persistent oscillations over the entire time window of our experimental observations (Fig. 2a). We perform a Fourier transform on subsections of the time trace with a sweeping window of size of $m = 20$ (Fig. 2a) and extract the intensity of the $\nu = 1/2$ peak as a function of the sweep position, n_{sweep} (Fig. 2b). The intensity of the $\nu = 1/2$ peak clearly exhibits two distinct decay timescales. At short times, we observe a rapid initial decay that corresponds to non-universal dephasing dynamics, whereas at late times we observe a slow decay. Only near the phase boundary ($\theta = 1.086\pi$) is the lifetime substantially decreased. We fit the slow decay to an exponential to extract a lifetime for the periodic order.

As shown in Fig. 2c, for $\theta = 1.034\pi$, this lifetime increases with the interaction time (τ_1) and eventually approaches the independently measured spin depolarization time $T_1^{\rho} \approx 60\ \mu s$. This demonstrates that, for sufficiently long interaction times, the observed periodic order is limited by only coupling to the environment[28]. We associate this with DTC order[9–12]. Within the DTC phase, the lifetime is essentially independent of θ, indicating exceptional robustness (Fig. 2d).

We examined whether the observed periodic order could arise from an accidental XY sequence[14] or from inhomogeneous dephasing resulting from the effective single-particle disorder in the dressed state basis. To avoid the former, τ_1 is always chosen as an integer multiple of $2\pi/\Omega_x$. For the latter, although it has been shown that disorder alone is insufficient for stabilizing a DTC phase in the absence of interactions[9–12], we verified this experimentally; implementing a rotary echo sequence that reduces such dephasing, we find no change in the lifetime of the DTC order and an enhancement in the subharmonic response at late times (see Methods and Extended Data Fig. 1). In principle, fast Markovian dephasing could also lead to apparent periodic order at extremely small values of $\theta - \pi$ by eliminating coherences along both $\hat{y}$ and $\hat{z}$, leaving only $\hat{x}$ polarization dynamics. In such a case, the decay rate of periodic order should increase quadratically with $\theta - \pi$. However, this explanation is inconsistent with the observed robustness of the lifetime of DTC order for a range of $\theta - \pi$ values (Fig. 2d) and the independently measured dephasing rate (see Methods).

To experimentally determine the DTC phase boundary, we focus on the long-time behaviour of the polarization time traces ($50 < n \leq 100$) and compute the 'crystalline fraction', which is defined as the ratio of the $\nu = 1/2$ peak intensity to the total spectral power, $f = |S(\nu = 1/2)|^2 / \sum_{\nu} |S(\nu)|^2$ (see Methods). Figure 3a shows f as a function of θ for two different interaction times. For weak interactions ($\tau_1 = 92$ ns), f has a maximum at $\theta = \pi$ and rapidly decreases as θ deviates by approximately 0.02π. However, for stronger interactions ($\tau_1 = 275$ ns), we observe a robust DTC phase, which manifests as a large crystalline fraction over a wide range $0.86\pi < \theta < 1.13\pi$. We associate a phenomenological phase boundary with $f = 10\%$ and observe that the boundary enlarges with τ_1, eventually saturating at $\tau_1 \approx 400$ ns (Fig. 3b). The phase boundary can also be visualized as the vanishing of the $\nu = 1/2$ peak and the simultaneous emergence of two incommensurate peaks (Fig. 3c).

The rigidity of the $\nu = 1/2$ peak can be qualitatively understood by constructing effective eigenstates of $2T$ Floquet cycles, including spin–spin interaction. We approximate the unitary time evolution over a single period as $U_T = R_y^{\theta} e^{-iH_{\mathrm{eff}}\tau_1}$ and solve for a self-consistent evolution using product states as a variational ansatz. To this end, we consider the situation in which a typical spin returns to its initial state after $2T$, $|\psi(0)\rangle \propto |\psi(2T)\rangle = e^{-i\theta S^y} e^{i\phi_i S^x} e^{-i\theta S^y} e^{-i\phi_i S^x} |\psi(0)\rangle$, and self-consistently determine the interaction-induced rotation angle $\phi_i \equiv \sum_j J_{ij}/r_{ij}^3 \langle S_j^x \rangle \tau_1 \approx \bar{J}_i \tau_1 \langle \psi(0)|S^x|\psi(0)\rangle$, where $|\psi(0)\rangle$ is the initial spin state and $\bar{J}_i = \sum_j J_{ij}/r_{ij}^3$ (see Methods). We expect ϕ_i to change sign after each Floquet cycle, because the average polarization $\langle \psi(0)|S_x|\psi(0)\rangle$ should be flipped. Intuitively, the self-consistent solution can be visualized as a closed path on the Bloch sphere (Fig. 3d), where each of the four arcs corresponds to one portion of the $2T$-periodic evolution. When $\theta = \pi$, such a solution always exists. More surprisingly, even for $\theta \neq \pi$ a closed path can still be found for sufficiently strong interactions, $|\bar{J}_i \tau_1| > 2|\theta_i - \pi|$; in such cases, the deviation in θ away from π is compensated by the dipolar interactions (Fig. 3d). We obtain a theoretical phase boundary by numerically averaging the self-consistent solution over both disordered spin positions and local fields. The resultant phase boundary is in reasonable agreement with the experimental observations for short to moderate interaction times τ_1, but overestimates the boundary at large τ_1 (dashed line, Fig. 3b; see Methods).

Finally, Fig. 4 demonstrates that the discrete time-translation symmetry can be further broken down to $\mathbb{Z}_3$ (refs 10–12, 29), resulting

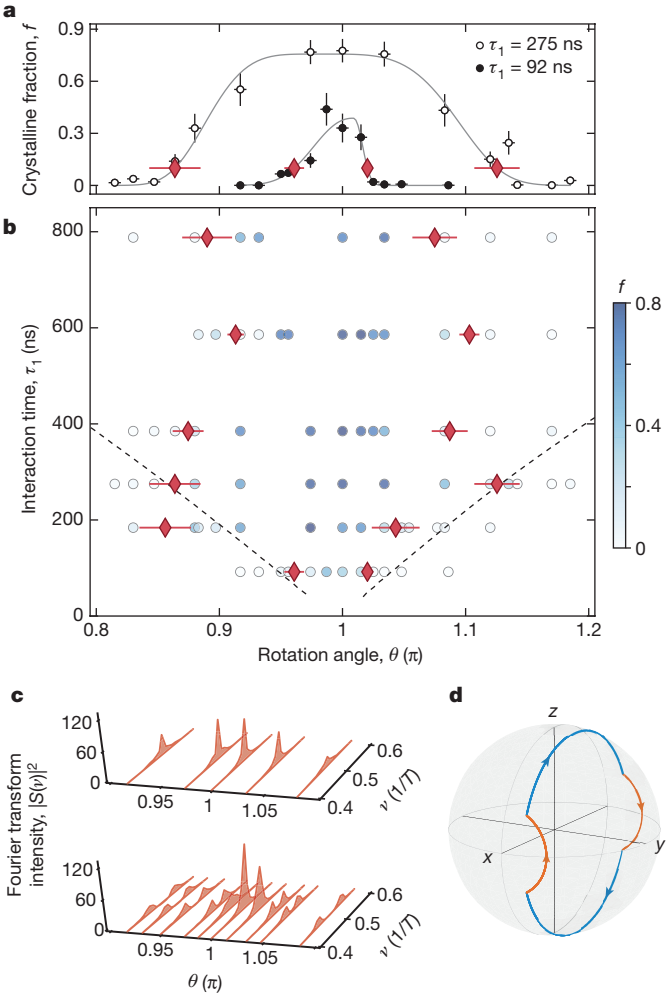

Figure 3 | Phase diagram and transition. a, **b**, Crystalline fraction f (**a**) and its associated phase diagram (**b**) as a function of θ and τ_1 obtained from a Fourier transform at late times ($50 < n \leq 100$). The red diamonds mark the phenomenological phase boundary, identified as a 10% crystalline fraction; horizontal error bars denote the statistical error (s.d.) from a super-Gaussian fit. In **a**, vertical error bars of data points (circles) are limited by the noise floor (see Methods) and horizontal error bars indicate the pulse uncertainty of 1%. Grey lines denote the fit to extract the phase boundary (see Methods). In **b**, the colours of the data points (circles) represent the extracted crystalline fraction at the associated parameter set. The dashed line corresponds to a disorder-averaged theoretical prediction for the phase boundary. Asymmetry in the boundary arises from an asymmetric distribution of rotation angles (see Methods). **c**, Evolution of the Fourier spectra as a function of θ for two different interaction times: $\tau_1 = 385$ ns (top) and $\tau_1 = 92$ ns (bottom). **d**, Bloch sphere indicating a single spin trajectory of the $2T$-periodic evolution under the long-range dipolar Hamiltonian (red) and global rotation (blue).

in DTC order at $\nu = 1/3$. Here, we utilize all three spin states of the nitrogen–vacancy centre. We begin with all of the spins polarized in the $|m_s = 0\rangle$ state and evolve under the bare dipolar Hamiltonian for a duration τ_1 (see Methods). Next, we apply two resonant microwave pulses, each of duration τ_2, first on the transition $|m_s = 0\rangle \rightarrow |m_s = -1\rangle$ and then on the transition $|m_s = 0\rangle \rightarrow |m_s = +1\rangle$. In combination, this sequence of operations defines a single Floquet cycle with period $T = \tau_1 + 2\tau_2$. As before, we measure the polarization $P(nT)$, which is defined as the population difference between the $|m_s = 0\rangle$ and $|m_s = -1\rangle$ states (Fig. 4a). When each of the applied microwaves corresponds to an ideal π pulse, this sequence realizes a cyclic transition with $\mathbb{Z}_3$ symmetry (Fig. 4b), which is explicitly broken by any change in the pulse duration. The Fourier spectra of $P(nT)$ for various pulse durations and for two different values of τ_1 are shown in Fig. 4c. With

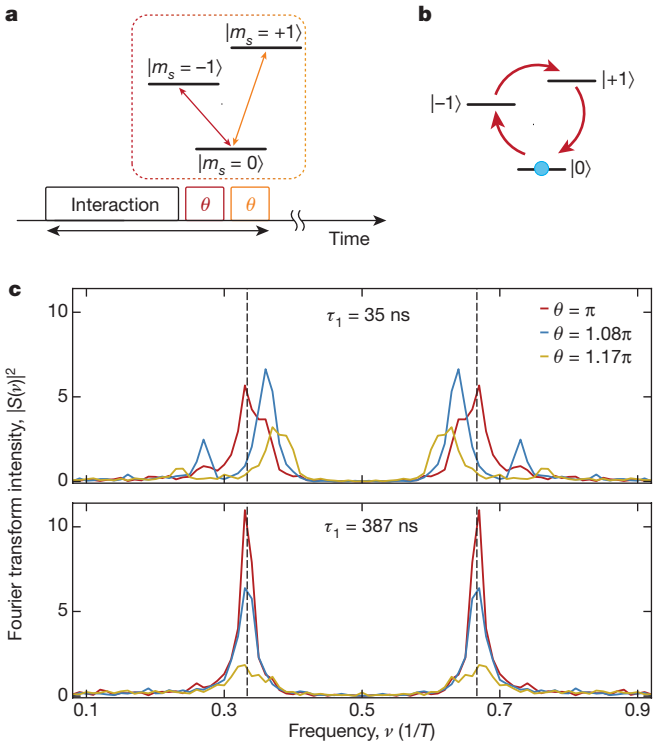

Figure 4 | $\mathbb{Z}_3$ discrete time-crystalline order. a, Experimental sequence demonstrating $3T$-periodic DTC order. A single Floquet cycle is composed of three operations: time evolution under a long-range dipolar Hamiltonian, and rapid microwave pulses for two different transitions. **b**, Visualization of the $3T$-periodicity in the polarization dynamics for the case of $\theta = \pi$. **c**, Fourier spectra of the polarization dynamics for two different interaction times and for three different rotation angles: $\theta = 1.00\pi$ (red), $\theta = 1.086\pi$ (blue) and $\theta = 1.17\pi$ (yellow). Dashed lines indicate $\nu = 1/3$ and $\nu = 2/3$.

weak interactions ($\tau_1 = 35$ ns), the position of the peaks is extremely sensitive to perturbations, but with sufficiently strong interactions ($\tau_1 = 387$ ns) the peaks are pinned to a value of $\nu = 1/3$ despite large perturbations, indicating the observation of a $\nu = 1/3$ DTC order. The lifetime of the observed $\nu = 1/3$ DTC order is shorter than that of the $\nu = 1/2$ DTC order, consistent with the presence of additional dynamics in the full dipolar Hamiltonian (see Methods). The ability for our system to exhibit stable period-tripling distinguishes it from bifurcations in driven, classical systems, in which period-tripling is typically accompanied by regions of chaos[30].

Our observation of DTC order cannot be simply explained within current theoretical frameworks based on either localization[9–12] or pre-thermalization[24,27]. In particular, our system with long-range dipolar interactions is not expected to be localized in either the static or the driven case. In the static case, it has previously been demonstrated that our system exhibits slow thermalization associated with critical dynamics[17]. In the driven case, the long-time evolution is governed by the average Hamiltonian $D \approx \sum_i \left(J_{ij}/r_{ij}^3\right) S_i^x S_j^x + (\theta - \pi)/T \sum_i S_i^y$, which likewise does not yield localized dynamics[16,31]. We further note that the effective Hamiltonian of the $\mathbb{Z}_3$ DTC phase includes not only Ising-type interactions but also spin exchange interactions, providing additional channels for thermalization (see Methods).

In principle, even in the absence of localization, time-crystalline order can persist for a long, but finite, pre-thermal timescale[24,27]. Within this timescale, the spin system relaxes to a pre-thermalized state, defined as the thermal ensemble of D with a temperature determined by the energy density of the initial state. Because our initially polarized state is effectively at infinite temperature with respect to D (owing to the anisotropy of the dipolar couplings), we do not expect to observe pre-thermal DTC order. This is in contrast to our actual observations, which show that the lifetime of the DTC order is limited by the depolarization time T_1^ρ, owing to coupling with the environment[28] (Fig. 2c). We have explicitly verified that the DTC order is not greatly affected by varying the initial polarization (see Methods). One possible explanation is that, owing to slow critical thermalization[17], the spins in our system do not reach even a pre-thermal state. Finally, the interplay between coherent interactions and dephasing in open systems at long times could also have a role. Detailed understanding of such mechanisms requires further theoretical investigation.

A number of remarkable phenomena in quantum dynamics have recently been observed in engineered many-body systems consisting of ten to a few hundred particles[3–6]. The observations that we have presented here indicate that robust DTC order can occur in large systems without fine-tuned interactions and disorder, even in the regime in which localization is nominally not expected to occur. Our work raises important questions about the role of localization, long-range interactions and coupling to the environment in driven systems, and opens up several new avenues for fundamental studies and potential applications. In particular, it should be possible to extend these studies to realize novel dynamical phases in more complex driven Hamiltonians, and to explore whether such phases can be used to create and stabilize coherent quantum superposition states for applications such as quantum metrology[18–20].

Online Content Methods, along with any additional Extended Data display items and Source Data, are available in the online version of the paper; references unique to these sections appear only in the online paper.

Received 21 October 2016; accepted 18 January 2017.

1. Adler, R. A study of locking phenomena in oscillators. *Proc. IRE* **34,** 351–357 (1946).
2. Cross, M. C. & Hohenberg, P. C. Pattern formation outside of equilibrium. *Rev. Mod. Phys.* **65,** 851–1112 (1993).
3. Schreiber, M. *et al.* Observation of many-body localization of interacting fermions in a quasirandom optical lattice. *Science* **349,** 842–845 (2015).
4. Langen, T. *et al.* Experimental observation of a generalized Gibbs ensemble. *Science* **348,** 207–211 (2015).
5. Smith, J. *et al.* Many-body localization in a quantum simulator with programmable random disorder. *Nat. Phys.* **12,** 907–911 (2016).
6. Kaufman, A. M. *et al.* Quantum thermalization through entanglement in an isolated many-body system. *Science* **353,** 794–800 (2016).
7. Wilczek, F. Quantum time crystals. *Phys. Rev. Lett.* **109,** 160401 (2012).
8. Sacha, K. Modeling spontaneous breaking of time-translation symmetry. *Phys. Rev. A* **91,** 033617 (2015).
9. Khemani, V., Lazarides, A., Moessner, R. & Sondhi, S. L. Phase structure of driven quantum systems. *Phys. Rev. Lett.* **116,** 250401 (2016).
10. Else, D. V., Bauer, B. & Nayak, C. Floquet time crystals. *Phys. Rev. Lett.* **117,** 090402 (2016).
11. von Keyserlingk, C., Khemani, V. & Sondhi, S. Absolute stability and spatiotemporal long-range order in Floquet systems. *Phys. Rev. B* **94,** 085112 (2016).
12. Yao, N. Y., Potter, A. C., Potirniche, I.-D. & Vishwanath, A. Discrete time crystals: rigidity, criticality, and realizations. *Phys. Rev. Lett.* **118,** 030401 (2017).
13. Childress, L. *et al.* Coherent dynamics of coupled electron and nuclear spin qubits in diamond. *Science* **314,** 281–285 (2006).
14. de Lange, G., Wang, Z. H., Ristè, D., Dobrovitski, V. V. & Hanson, R. Universal dynamical decoupling of a single solid-state spin from a spin bath. *Science* **330,** 60–63 (2010).
15. Doherty, M. W. *et al.* The nitrogen-vacancy colour centre in diamond. *Phys. Rep.* **528,** 1–45 (2013).
16. Anderson, P. W. Absence of diffusion in certain random lattices. *Phys. Rev.* **109,** 1492–1505 (1958).
17. Kucsko, G. *et al.* Critical thermalization of a disordered dipolar spin system in diamond. Preprint at https://arxiv.org/abs/1609.08216 (2016).
18. Deutsch, C. *et al.* Spin self-rephasing and very long coherence times in a trapped atomic ensemble. *Phys. Rev. Lett.* **105,** 020401 (2010).
19. Rey, A. M., Jiang, L., Fleischhauer, M., Demler, E. & Lukin, M. D. Many-body protected entanglement generation in interacting spin systems. *Phys. Rev. A* **77,** 052305 (2008).
20. Cappellaro, P. & Lukin, M. D. Quantum correlation in disordered spin systems: applications to magnetic sensing. *Phys. Rev. A* **80,** 032311 (2009).
21. Waugh, J., Huber, L. & Haeberlen, U. Approach to high-resolution NMR in solids. *Phys. Rev. Lett.* **20,** 180–182 (1968).
22. Basko, D., Aleiner, I. & Altshuler, B. Metal–insulator transition in a weakly interacting many-electron system with localized single-particle states. *Ann. Phys.* **321,** 1126–1205 (2006).
23. Nandkishore, R. & Huse, D. A. Many-body localization and thermalization in quantum statistical mechanics. *Annu. Rev. Condens. Matter Phys.* **6,** 15–38 (2015).

24. Abanin, D. A., De Roeck, W. & Huveneers, F. Exponentially slow heating in periodically driven many-body systems. *Phys. Rev. Lett.* **115,** 256803 (2015).
25. Bruno, P. Impossibility of spontaneously rotating time crystals: a no-go theorem. *Phys. Rev. Lett.* **111,** 070402 (2013).
26. Watanabe, H. & Oshikawa, M. Absence of quantum time crystals. *Phys. Rev. Lett.* **114,** 251603 (2015).
27. Else, D. V., Bauer, B. & Nayak, C. Pre-thermal time crystals and Floquet topological phases without disorder. Preprint at https://arxiv.org/abs/1607.05277 (2016).
28. Choi, J. *et al.* Depolarization dynamics in a strongly interacting solid-state spin ensemble. *Phys. Rev. Lett.* (in the press).
29. von Keyserlingk, C. W. & Sondhi, S. L. Phase structure of one-dimensional interacting Floquet systems. II. Symmetry-broken phases. *Phys. Rev. B* **93,** 245146 (2016).
30. Li, T.-Y. & Yorke, J. A. Period three implies chaos. *Am. Math. Mon.* **82,** 985–992 (1975).
31. Yao, N. Y. *et al.* Many-body localization in dipolar systems. *Phys. Rev. Lett.* **113,** 243002 (2014).

Acknowledgements We thank D. A. Huse, S. L. Sondhi, A. Vishwanath and M. Zaletel for discussions, and N. P. De Leon and P. C. Maurer for fabricating the diamond nanobeam and experimental help. This work was supported in part by CUA, NSSEFF, ARO MURI, Moore Foundation, Harvard Society of Fellows, Princeton Center for Theoretical Science, Miller Institute for Basic Research in Science, Kwanjeong Educational Foundation, Samsung Fellowship, Purcell Fellowship, NSF PHY-1506284, NSF DMR-1308435, Japan Society for the Promotion of Science KAKENHI (No. 26246001), LDRD Program of LBNL under US DOE Contract No. DE-AC02-05CH11231, EU (FP7, Horizons 2020, ERC), DFG, SNF, Volkswagenstiftung and BMBF.

Author Contributions S.C. and M.D.L. developed the idea for the study. J.C., R.L. and G.K. designed and conducted the experiment. H.S., S.O., J.I. and F.J. fabricated the sample. S.C., H.Z., V.K., C.v.K., N.Y.Y. and E.D. conducted the theoretical analysis. All authors discussed the results and contributed to the manuscript.

Author Information Reprints and permissions information is available at www.nature.com/reprints. The authors declare no competing financial interests. Readers are welcome to comment on the online version of the paper. Correspondence and requests for materials should be addressed to M.D.L. (lukin@physics.harvard.edu).

Reviewer Information *Nature* thanks D. A. Huse and the other anonymous reviewer(s) for their contribution to the peer review of this work.

METHODS

Experimental details. Our sample and experimental set-up have been previously described[17]. We utilize a diamond sample containing a high concentration (about 45 p.p.m.) of nitrogen–vacancy (NV) centres, corresponding to an average NV–NV separation of 5 nm. For a single crystalline orientation of NV centres, selected by applying an external magnetic field, this corresponds to an average separation of 8 nm, resulting in a typical dipolar interaction strength of $2\pi \times 105$ kHz. The system exhibits strong on-site energy disorder, owing to the effects of lattice strain, the random position of NV centres and the presence of scattered paramagnetic impurities (consisting mainly of P1 centres and ^{13}C nuclear spins). For each NV, the effective random field Δ_i is therefore a function of its local environment, including interaction effects of neighbouring NV centres. This results in an approximately Gaussian distribution with standard deviation $W = 2\pi \times 4.0$ MHz. We extract W by measuring the linewidth of an electron spin resonance (ESR) spectrum with sufficiently weak microwave driving strength to avoid power broadening. To control the experimental probe volume, we fabricate a diamond nanobeam structure (about 300 nm × 300 nm × 20 μm) and confocally address a region of approximately 300-nm diameter using a green laser (532 nm). This realizes an effective three-dimensional excitation volume containing about 10^6 NV centres. By applying an external magnetic field along one of the diamond crystal axes, we spectrally isolate one group of NV centres and selectively address an effective two-level system between the $|m_s = -1\rangle$ and $|m_s = 0\rangle$ spin states via coherent microwave radiation. The addition of a microwave in-phase/quadrature (IQ) mixer allows for arbitrary rotations around any linear combination $\hat{x}$ and $\hat{y}$.

Experimental sequence. Initial polarization of NV centres into $|m_s = 0\rangle$ is performed via laser illumination at a wavelength of 532 nm, a power of 50 μW and a duration of 100 μs. Subsequent application of a microwave $-\pi/2$ pulse along the $\hat{y}$ axis is used to coherently rotate the spin ensemble into $|+\rangle = (|m_s = 0\rangle + |m_s = -1\rangle)/\sqrt{2}$. The spins are then subjected to continuous driving at a Rabi frequency of $2\pi \times 54.6$ MHz along the $\hat{x}$ axis for a duration τ_1. This so-called spin-locking technique suppresses two-spin (flip-flip and flop-flop) processes, owing to energy conservation, and decouples spins from their environment[17]. In our sample, this technique leads to spin lifetimes of $T_1^{\rho} \approx 60$ μs (ref. 28). Finally, we apply a short microwave pulse along the $\hat{y}$ axis over an angle $\theta \approx \pi$. We repeat this Floquet cycle with various values of θ, controlled by changing the Rabi driving strength and the pulse duration. The imperfection in microwave manipulations (for initialization into $|+\rangle$ and rotation angles θ) amounts to 0.9% and arises from a combination of spatial inhomogeneity of the driving field (0.8%) and on-site potential disorder (0.6%). Following a coherent time evolution, the spin state of the NV ensemble is optically detected by applying a final $\pi/2$ pulse along the $\hat{y}$ axis and measuring the population difference in the $|m_s = 0\rangle$ and $|m_s = -1\rangle$ basis. The polarization is defined as $P = \mathcal{P}_0 - \mathcal{P}_{-1}$, with $\mathcal{P}_a$ denoting the population in spin state a, and is determined by calibrating the NV fluorescence using a Rabi oscillation contrast measurement. To avoid heating of the sample, which would result in drifts in the Rabi frequency, a waiting time of 600–900 μs is implemented before the sequence is repeated. The minimum spacing between microwave pulses is maintained at 1 ns.

To understand the effect of different initial states on the DTC phase, we replaced the initial $-\pi/2$ pulse with a $-\pi/3$ pulse. This results in the preparation of a global spin state, which is rotated from the $\hat{x}$ axis by $\pi/6$. Despite this change, the measured lifetime of the DTC order (47.6 ± 2.4 μs) agrees well with that of the polarized spin state (49.2 ± 3.3 μs), demonstrating that DTC order is insensitive to the initial state.

Experimental identification of phase boundary. To identify the position of the phase boundary in our experiment, we define the crystalline fraction f as $f = |S(\nu = 1/2)|^2 / \sum_\nu |S(\nu)|^2$. Error bars in f are calculated via error propagation in consideration of the noise floor in the Fourier spectrum; each measured spectrum contains a background noise level σ_n, resulting in the following variation in f:

$$\delta f = f \sqrt{\left[\frac{\sigma_n}{|S(\nu = 1/2)|^2}\right]^2 + \left[\frac{N\sigma_n}{\sum_\nu |S(\nu)|^2}\right]^2 - \frac{2N\sigma_n^2}{|S(\nu = 1/2)|^2 \sum_\nu |S(\nu)|^2}}$$

where $N = 50$ is the number of points in the Fourier spectrum. This gives rise to an uncertainty in the crystalline fraction: $f \in [f - \delta f, f + \delta f]$ (Fig. 3a). To extract the phase boundary, we use a phenomenological, super-Gaussian function

$$F_{\tau_1}(\theta) = \begin{cases} f_{\tau_1}^{\max} \exp\left[-\frac{1}{2}\left(\frac{|\theta - \theta_0|}{\sigma_-}\right)^p\right] & \theta \le \theta_0 \\ f_{\tau_1}^{\max} \exp\left[-\frac{1}{2}\left(\frac{|\theta - \theta_0|}{\sigma_+}\right)^p\right] & \theta \ge \theta_0 \end{cases}$$

where $\sigma_\pm$, θ_0 and p are the characteristic width, central position and the power of the super-Gaussian fit, and $f_{\tau_1}^{\max}$ is the maximum value of the crystalline fraction for a given duration τ_1. The proposed function naturally captures the observed asymmetry in the phase boundary. We define the phase boundary as the rotation angle $\theta_\pm$ at which $F_{\tau_1}(\theta_\pm) = 0.1$; that is, $\theta_\pm = \theta_0 \pm \sigma_\pm \left[2\ln\left(f_{\tau_1}^{\max}/0.1\right)\right]^{1/p}$. Errors in the phase boundary are derived from the uncertainties in the fit.

Theoretical description. As a variational ansatz, we consider the time evolution of a homogeneous product state of the form $|\Psi\rangle = |\psi_0\rangle^{\otimes N}$ with $|\psi_0\rangle = \cos(\theta_0/2)|+\rangle + \sin(\theta_0/2)e^{i\phi_0}|-\rangle$, where $|\pm\rangle = (|m_s = 0\rangle \pm |m_s = -1\rangle)/\sqrt{2}$. The qualitative behaviour does not change even if we allow spins to be oriented in different directions. An approximate eigenstate for the time evolution over two periods is obtained by solving the equation for a single spin, $|\psi_0\rangle = e^{-i\theta S^y} e^{i\phi_i S^x} e^{-i\theta S^y} e^{-i\phi_i S^x} |\psi_0\rangle$, with a self-consistently determined $\phi_i = \bar{J}_i \langle\psi_0|S^x|\psi_0\rangle$, where $\bar{J}_i = \sum_j J_{ij}/r_{ij}^3$ is the total strength at site i. The sign of ϕ_i is flipped in the second evolution because the spin polarization along the $\hat{x}$ direction alternates in each cycle. Note that we have ignored the effects of the on-site disorder potential Δ_i, interactions during global rotations and rotations induced by Ω_x. This is justified because of the high microwave driving strength $\Omega_{x(y)} \gg W$ and $\Omega_x \tau_1$ being integer multiples of 2π. (The effects of on-site disorder are fully included in the numerical computations.) A non-trivial solution ($\theta_0 \neq \pm\pi$) is obtained if the first two rotations result in a vector that is rotated by π along the $\hat{y}$ axis (Fig. 3d), which is satisfied when $\phi_0 = m\pi - \phi_i/2$, with $m \in \mathbb{Z}$ and $\cot\theta_0 = -(-1)^m \tan(\theta/2)\sin(\phi_i/2)$. Solving for $\cos^2\theta_0$ yields

$$\cos^2\theta_0 = \frac{\tan^2(\theta/2)\sin^2(\phi_i/2)}{1 + \tan^2(\theta/2)\sin^2(\phi_i/2)}$$

Using $\phi_i = \bar{J}_i \tau_1 \cos\theta_0$, it can be shown that a solution exists only when $|\tan(\theta/2)\bar{J}_i\tau_1/4| > 1$, implying that $|\theta - \pi| < |\bar{J}_i\tau_1/2|$ in the vicinity of $\theta \approx \pi$. The linear dependence of the phase boundary is consistent with the numerically extracted phase diagram in ref. 12. As long as a solution exists, small variations in θ correspond to a smooth deformation of the closed trajectory. Therefore, the existence of such a closed path stabilizes the time-crystalline phase. We emphasize that such a $2T$-periodic path is a consequence of interactions; without the change of sign in ϕ_i, the eigenstates of the unitary evolution over one or two periods coincide and, therefore, unless the rotation angle is fine-tuned, T-periodic motion cannot be broken into a $2T$ period. The eigenstates of unitary evolution over one period can be obtained as even and odd linear combinations, $(|\Psi\rangle \pm e^{-i\epsilon}U_1|\Psi\rangle)/\sqrt{2}$, where $U_1 = \otimes_i (e^{-i\theta S_i^y} e^{-i\phi_i S_i^x})$ and the quasi-energy eigenvalue is given by $e^{i\epsilon} = \pm(\langle\Psi|(U_1)^2|\Psi\rangle)^{1/2}$.

To estimate the phase boundary, we numerically solve the self-consistency equation. Here, we include the effects of on-site disorder potential Δ_i in all four rotations and the disorder in $\bar{J}_i$ that arises from the random positions of NV centres. The distribution of $\bar{J}_i$ is simulated for 1,000 spins, which are randomly distributed in three dimensions with an average separation r_0 and minimum cutoff distance $r_{\min} = 3$ nm (limited by NV–NV electron tunnelling[28]). Instead of $\cos\theta_0$, we solve for a self-consistent distribution for $\cos\theta_0$, where $\langle S^x\rangle$ is defined as the mean of the distribution. The average order parameter $\langle\cos^2\theta_0\rangle$ is computed for various values of τ_1 and θ and compared with a threshold value of 0.1 to identify the phase boundary. The experimental and numerical phase boundaries are asymmetric about $\theta = \pi$. We attribute this asymmetry to the inherently asymmetric distribution of the effective rotation angle, $\theta_i \approx \tau_2\sqrt{\Omega_y^2 + \Delta_i^2 + \bar{J}_i^2}$, which causes the transition to occur earlier for positive deviations $\theta - \pi$.

Although we assumed ϕ_i to be a classical variable in this analysis, the interaction-induced rotation angle is an operator $\hat{\phi}$ that exhibits quantum fluctuations and leads to non-trivial quantum dynamics. Under such dynamics, spins get entangled, resulting in mixed-state density matrices. These effects cannot be ignored in the case of long interaction times, effectively limiting the present description. We believe that the diminished range of θ in the experimentally obtained phase diagram (Fig. 3b) is related to this effect.

Rotary echo sequence. Certain features similar to DTC order could potentially arise from spatially inhomogeneous microwave driving along the $\hat{x}$ axis during the spin-locking sequence. This leads to variations in the effective, single-particle disorder in the dressed state basis, which could give rise to an effective self-correcting dynamical decoupling that might resemble DTC order[14]. In particular, in the spin-locking sequence, spins precess along the axis $[\Omega_x(r_i) + \bar{J}_i]\hat{x} + \Delta_i\hat{z}$, with effective Rabi frequency $\Omega_{x,i}^{\text{eff}} = \sqrt{[\Omega_x(r_i) + \bar{J}_i]^2 + \Delta_i^2}$, where $\Omega_x(r_i)$ is the spatially inhomogeneous Rabi frequency, $\bar{J}_i$ is the mean-field Ising interaction and Δ_i characterizes the quasi-static on-site disorder. In the case of strong driving ($\Omega_x \gg \Delta_i, \bar{J}_i$), this precession axis is determined by Ω_x and spins undergo dephasing dominated by global microwave inhomogeneities. If the net rotation during one spin-locking cycle is an odd integer multiple of π, then this could accidentally lead to an XY sequence[14] that may result in $2T$-periodicity. In our measurements, we always choose τ_1 as an integer multiple of $2\pi/\Omega_x$ to minimize such effects.

Although it has been shown theoretically that disorder alone is insufficient (in the absence of interactions) for stabilizing DTC order[9–12], to experimentally demonstrate that the accidental decoupling is not responsible for the observed DTC ordering, we implement a 'rotary echo' sequence, wherein after half the interaction time τ_1 the microwave driving is flipped from Ω_x to $-\Omega_x$ (Extended Data Fig. 1a). In the limit of strong driving, such a sequence eliminates the phase acquired between the two dressed states for each spin, regardless of the exact value of Ω_x. As shown in Extended Data Fig. 1b, the lifetimes of the DTC order are nearly identical between the cases of the rotary echo and continuous $+\hat{x}$ driving. Moreover, the rotary echo spin polarization maintains a larger amplitude at late times, excluding the possibility of self-correcting dynamical decoupling as the origin of the observed DTC order.

Markovian dephasing effects on DTC order. The presence of the subharmonic peak at $\nu = 1/2$ at small values of $\theta - \pi$ can, in principle, also be explained on the basis of fast Markovian dephasing in the dressed state basis. Indeed, for sufficiently fast dephasing, coherences along both $\hat{y}$ and $\hat{z}$ will be eliminated after each rotation, R^{θ}_{y}. Therefore, the only evolution that remains is the population dynamics along $\hat{x}$, which exhibits $2T$-periodicity from the alternating sign. Microscopically, such strong dephasing could potentially originate from either dipolar interactions between the spins or from coupling to an external (Markovian) environment.

Intuitively, the result of such dephasing can be understood as an 'effective' projective measurement of polarization along $\hat{x}$ in each Floquet cycle, reminiscent of the quantum Zeno effect. To quantify and distinguish such dephasing-induced subharmonic rigidity, we consider the dynamics (over one Floquet period) of a single spin undergoing Markovian dephasing, with super-operator $\hat{\mathcal{D}}[\rho] = -\gamma(\rho - 4S^x\rho S^x)/2$ and dephasing rate γ. Assuming $\theta - \pi \ll 1$, evolution falls into two well-known limits. In the under-damped limit (weak dephasing), $S(\nu)$ has two Lorentzian peaks at $\nu = \pm\eta$ with a linewidth set by $\gamma\tau_1$, where τ_1 is the spin-locking duration and $\cos(2\pi\eta) = \cos\theta(1 + e^{\gamma\tau_1})/2$. In the over-damped limit (strong dephasing), $S(\nu)$ (at late times) has a peak at $\nu = 1/2$ with a linewidth (in Floquet units) of

$$\Gamma \approx \frac{(\theta - \pi)^2}{2\tanh(\gamma\tau_1/2)} \tag{1}$$

These over-damped oscillations of the spin polarization exhibit sign flips between the even and odd cycles, leading to a subharmonic Fourier response that is reminiscent of DTC order.

Although strong Markovian dephasing can indeed result in a $\nu = 1/2$ subharmonic peak, we observe three distinct experimental signatures that clearly show that our observations are not governed by this effect. First, the linewidth Γ (equation (1)) of the subharmonic peak should be quadratically sensitive to the deviation of θ from π. This is in stark contrast with our experimental observations shown in Fig. 2d, wherein this linewidth Γ is essentially independent of θ within the DTC phase. Second, according to the dephasing model (equation (1)), the lifetime of the $3T$-periodic DTC order is expected to be longer than that of the $2T$-periodic DTC order owing to enhanced dephasing (from a lack of spin-locking) in the bare basis[28]. However, we observe the exact opposite behaviour. Finally, Markovian dephasing requires an effective environment with a relatively fast, sub-microsecond correlation time. This is also inconsistent with our experimental observations. In particular, we performed Rabi oscillation decay measurements with a rotary echo sequence, resulting in a lower bound of 1.5 μs on the Markovian dephasing time T_2. This time scale includes contributions from static on-site disorder and interactions, so the Markovian dephasing rate is, in fact, much slower than this. Indeed, we independently extracted the typical timescales of disorder fluctuations in our system[17], and found that they are similar (60 μs) to the depolarization timescale under spin-locking dynamics. Effects resulting from such slow dephasing should be completely negligible within a typical Floquet period. Therefore, we conclude that fast dephasing alone does not explain the observed DTC order.

At the same time, in the time crystalline order description based on interacting spin models[9–12], the time-crystalline order is expected to be robust and is not expected to exhibit any functional dependence on the angle θ, in complete agreement with experimental observations. This is also the case for our self-consistent description. We finally note that the interplay between coherent interactions and dephasing could potentially have a role in stabilizing DTC order at longer interaction times. A detailed understanding of such mechanisms requires further theoretical investigation.

Derivation of effective Hamiltonian for the $\mathbb{Z}_3$ symmetry breaking phase. Using microwave driving resonant with two different transitions (Fig. 4a), we realize dynamics involving all three spin states and observe robust $3T$-periodic time-crystalline order. The unitary matrix of the time evolution during the fundamental period T is

$$U_3 = \exp\left[-i\frac{\theta}{2}\sum_i (\sigma^i_{+1,0} + \sigma^i_{0,+1})\right]\exp\left[-i\frac{\theta}{2}\sum_i (\sigma^i_{-1,0} + \sigma^i_{0,-1})\right]\exp(-iH_2\tau)$$

where $\sigma^i_{a,b} \equiv |m_s = a\rangle\langle m_s = b|$ for spin i and $H_2 = H_{\mathrm{dis}} + H_{\mathrm{int}}$ is the effective Hamiltonian of NV centres for all three spin states, including on-site disorder potentials $H_{\mathrm{dis}} = \sum_i \Delta^+_i \sigma^i_{+1,+1} + \Delta^-_i \sigma^i_{-1,-1}$ and dipolar interactions for spin-1 particles[17]

$$H_{\mathrm{int}} = \sum_{ij}\frac{J_{ij}}{r^3_{ij}}\left[-\frac{\sigma^i_{+1,0}\sigma^j_{0,+1} + \sigma^i_{-1,0}\sigma^j_{0,-1} + \mathrm{h.c.}}{2} + (\sigma^i_{+1,+1} - \sigma^i_{-1,-1})(\sigma^j_{+1,+1} - \sigma^j_{-1,-1})\right]$$

This Hamiltonian is obtained in the rotating frame under the secular approximation. The Hamiltonian H_2 conserves the total population in any of the three spin states: $\mathcal{P}_a = \sum_i \sigma^i_{aa}$ with $a \in \{0, \pm 1\}$. If each microwave pulse realizes a π pulse ($\theta = \pi$), then their combination results in a cyclic transition $R^{\pi}_3 : |m_s = +1\rangle \mapsto -i|m_s = 0\rangle \mapsto -|m_s = -1\rangle \mapsto |m_s = +1\rangle$ and the population $\mathcal{P}_a$ becomes periodic over three periods. Under such evolution, the effective Hamiltonian over three periods is given by $D^{\pi}_3 = \left[H_2 + \left(R^{\pi}_3\right)^{-1} H_2 R^{\pi}_3 + \left(R^{\pi}_3\right)^{-2} H_2 \left(R^{\pi}_3\right)^2\right]/3$, in which on-site disorders average to zero, and the interactions are modified to

$$D^{\pi}_3 = \sum_{ij}\frac{J_{ij}}{r^3_{ij}}\left[\sum_a \sigma^i_{aa}\sigma^j_{aa} - \frac{1}{3}\sum_{a\neq b}\sigma^i_{ab}\sigma^j_{ba}\right]$$

The first term describes Ising-like interactions that shift energy when any pair of spins are in the same state, and the second term corresponds to spin-exchange interactions that allow polarization transport. These additional exchange interactions may lead to a shorter lifetime of the DTC order compared to that of the $\nu = 1/2$ DTC order. For small perturbations in the microwave pulse angle $\epsilon = \theta - \pi$, the effective dynamics, to leading order, are governed by

$$D^{\pi+\epsilon}_3 \approx D^{\pi}_3 + \frac{\epsilon}{3\tau}\sum_j (\sigma^j_{+1,0} + \sigma^j_{-1,0} + i\sigma^j_{+1,-1} + \mathrm{h.c.})$$

which explicitly breaks the conservation laws for $\mathcal{P}_a$.

Data availability. The data generated during this study are available from the corresponding author on reasonable request.

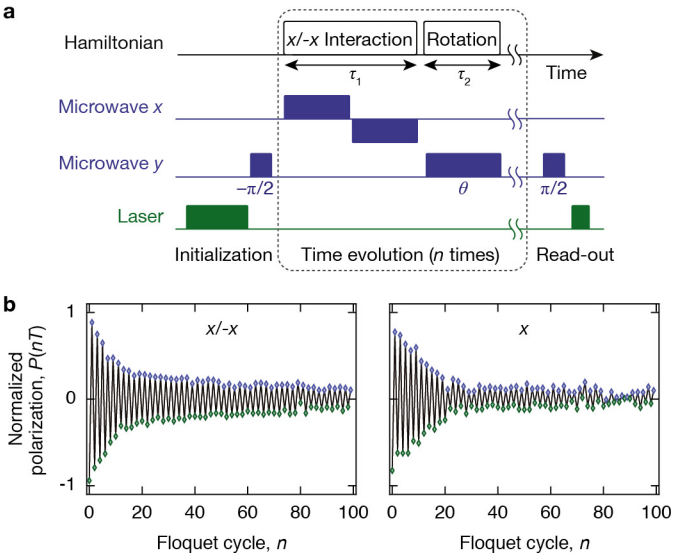

Extended Data Figure 1 | Effect of rotary echo sequence. a, Experimental sequence: during the interaction interval τ_1, the phase of the microwave driving along $\hat{x}$ is inverted after $\tau_1/2$. **b**, Comparison of time traces of $P(nT)$, measured at even (green) and odd (blue) integer multiples of T, in the presence (left) and absence (right) of an $\hat{x}/-\hat{x}$ rotary echo sequence at similar τ_1 and θ (left, $\tau_1 = 379$ ns, $\theta = 0.979\pi$; right, $\tau_1 = 384$ ns, $\theta = 0.974\pi$). The rotary echo leads to more pronounced $2T$-periodic oscillations at long time. The microwave frequencies used in the rotary echo sequence are $\Omega_x = 2\pi \times 52.9$ MHz and $\Omega_y = 2\pi \times 42.3$ MHz.